STABILIZATION OF A BALLOON BORNE ASTRONOMICAL INSTRUMENT

JAMES F. McNERNEY
AND
PAUL W. DANELL

STABILIZATION OF A BALLOON BORNE ASTRONOMICAL INSTRUMENT

by

JAMES FRANCIS McNERNEY
Lieutenant, United States Navy

and

PAUL WILLIE DANELL
Lieutenant, United States Navy

SUBMITTED IN PARTIAL FULFILLMENT OF THE REQUIREMENTS FOR THE DEGREE OF MASTER OF SCIENCE

at the

MASSACHUSETTS INSTITUTE OF TECHNOLOGY

1959

STABILIZATION OF A BALLOON BORNE

ASTRONOMICAL INSTRUMENT

by

James F. McNerney

Paul W. Danell

Submitted to the Department of Aeronautics and Astronautics on May 25, 1959, in partial fulfillment of the requirements for the degree of Master of Science.

ABSTRACT

Astronomical observation from the surface of the earth has been limited by image distortion caused by the earth's atmosphere. The recent development of high altitude balloons which can carry heavy loads has made it possible to transport astronomical instruments above a large portion of the atmosphere.

In order to perform many astronomical experiments, the astronomical instrument must maintain a direction in space, generally with reference to the fixed stars. Stabilization is the process by which this orientational control is achieved.

The stabilization problem is defined in order to determine geometrical relationships which may be instrumented. A method of instrumentation of a specific astronomical instrument is proposed. In order to determine the feasibility of this method, a stabilization system was constructed and used to track an artificial star in the laboratory. The static and dynamic performance of this system is analyzed. Improvements on the system and problems encountered are discussed.

Thesis Supervisor: Winston R. Markey
Title: Assistant Professor of
Aeronautics and Astronautics

May 25, 1959

Professor Alvin Sloane
Secretary of the Faculty
Massachusetts Institute of Technology
Cambridge 39, Massachusetts

Dear Professor Sloane:

In accordance with the regulations of the faculty, we hereby submit a thesis entitled Stabilization of a Balloon Borne Astronomical Instrument in partial fulfillment of the requirements for the degree of Master of Science in Aeronautical Engineering.

James F. McNerney

Paul W. Danell

ACKNOWLEDGEMENT

The authors gratefully acknowledge the advice and assistance of their thesis supervisor, Professor Winston Markey. Many members of the staff of the M. I. T. Instrumentation Laboratory were of great help to us. In particular we should like to thank Mr. John Hovorka and Mr. H. Phillip Whitaker. Special thanks go to Dr. Herbert French of the British Admiralty for his technical labors in our behalf.

CONTENTS

OBJECT

To investigate the theoretical and practical aspects of the stabilization of an astronomical instrument carried by a high altitude balloon.

CHAPTER 1

INTRODUCTION

1-1 THE STABILIZATION PROBLEM

Figure 1.1 illustrates the geometry of the proposed stabilization problem. An astronomical instrument consisting of a case and a sensing element is supported by a base in a manner to be discussed. The line of sight to the object is defined to be the line determined by the center of mass of the instrument and the centroid of the object. The optical axis of the instrument is shown to be misaligned with respect to the line of sight. The sensing element could be a photographic plate, spectroscope, or other measuring device. It is mounted on the instrument case so that rotation of the sensing element with respect to the instrument case about the optical axis of the instrument is possible and translation of the sensing element with respect to the instrument case normal to the optical axis of the instrument is not possible.

Execution of the experiment requires stabilization of the image of the object with respect to a sensing element co-ordinate system during the period of observation. Stabilization is required because the base (balloon system) may be rotating and interfering moments may be acting on the instrument. This base rotation is referred to a co-ordinate system fixed with respect to the stars.

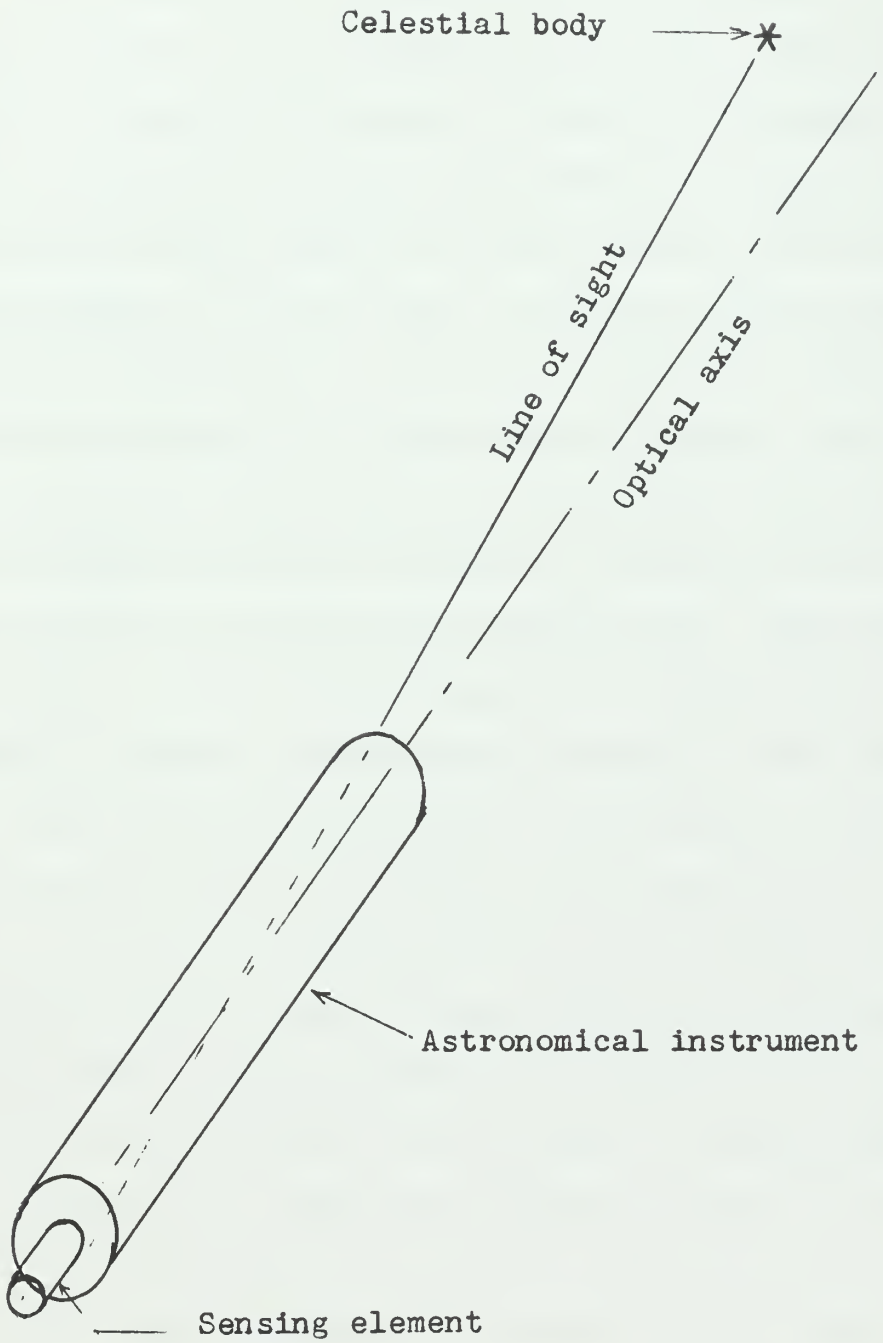

Figure 1.1 Illustration of the geometry of the stabilization problem.

Image motion, then, is caused by roll, pitch, and yaw motion of the base referred to a star-fixed co-ordinate system.

Four stabilization methods could be instrumented. If the optical system is fixed with respect to the instrument case, image stabilization is achieved by control of the angular motion of the instrument. In this case the angle between the optical axis and the line of sight, and the rotation of the sensing element co-ordinate system about the line of sight with respect to the star-fixed co-ordinate system are controlled to within the tolerance set for a particular experiment. Under these conditions two methods of instrumentation are possible: either mechanically fix the instrument case, and hence the optical axis, to the base and stabilize the base; or support the instrument case from the base with gimbals and stabilize the instrument case. Both methods would require reaction torques acting on the instrument case to be generated in response to sensed angular deviations. If the mass of the base is large compared with the mass of the instrument, the first method would require uneconomically larger torques than the second. Also, if the mass of the sensing element is small compared with the mass of the instrument case and base combination, roll stabilization of the image would be best accomplished by stabilizing only the sensing element in roll with respect to the star-fixed co-ordinate system.

The second two stabilization methods are based on the assumption that the optical system can be rotated with respect to the instrument case. Here image stabilization is achieved by roll stabilization and by angular control of the axis of symmetry of the convergent bundle of light rays that form the image, here called the optical axis of the image. Again two methods of instrumentation are possible. First, the instrument case may be mechanically fixed to the base, in which case the two

control processes necessary to affect stabilization are: alignment of the optical axis of the image with respect to the Z axis of the sensing element co-ordinate system; and roll stabilization of the image about this Z axis. The second possibility is to support the instrument case from the base with gimbals and execute three control processes: tracking of the line of sight using a tracker mounted on the instrument case; alignment of the optical axis of the image as was described; and roll stabilization of the image about the Z axis of the sensing element co-ordinate system. If the instrument case is fixed to the base, alignment of the axis of the convergent bundle of light rays that form the image with respect to the Z axis will be difficult if the base is rotating through large angles.

Two of the previously discussed image stabilization methods require gimbaling of the instrument case with respect to the base. Gimbaling of the case and rotation of the optical axis of the image with respect to the case will probably permit more accurate control of the image.

1-2 INSTRUMENTATION OF THE STABILIZATION PROBLEM

Three of the four stabilization methods discussed require tracking of the line of sight to the subject. Figure 1.2 is an illustrative functional diagram that shows the tracking control process. It is assumed for illustrative purposes that the instrument case is gimbaled with respect to the base about one axis only. An object tracker is mounted on the instrument case. This tracker generates a signal which is proportional to the angle between the line of sight and the tracking line. The tracking line may be the optical axis of the instrument or the optical axis of the tracker, both of which are shown fixed with respect

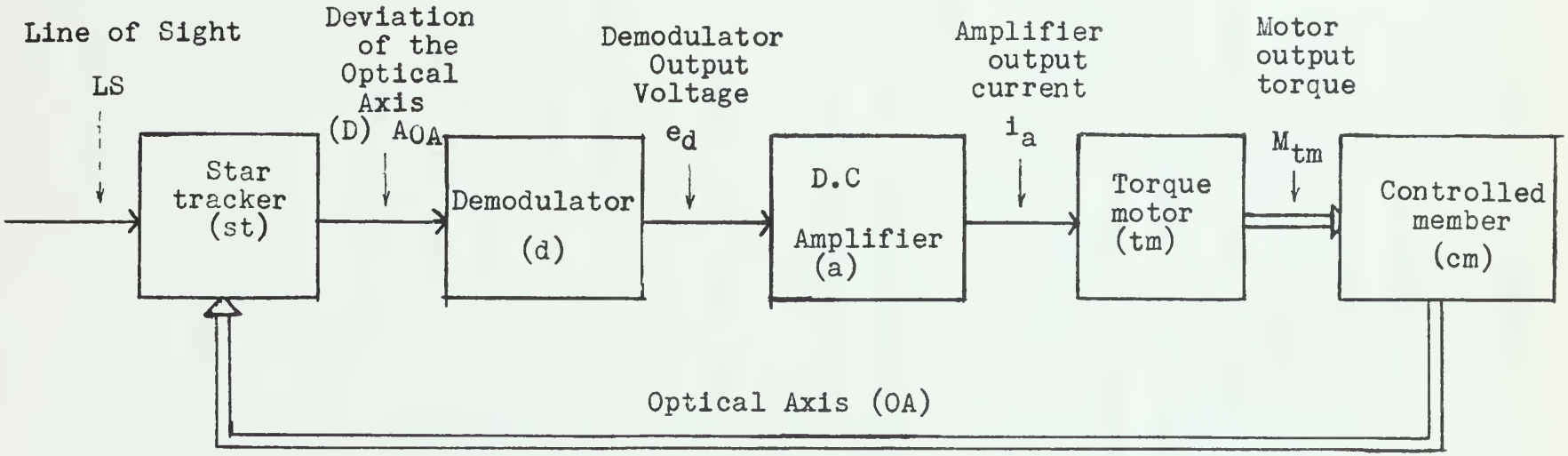

Figure 1.2 Illustrative functional diagram of a single axis telescope stabilization system.

to the instrument case. The tracking correction signal is processed electronically to produce a gimbal drive motor current. The drive motor torque which results from this current rotates the instrument case about the gimbal bearing axis until the tracking correction signal is nulled. Static accuracy of the tracking loop is a function of the individual component inaccuracies. In the presence of base motion, stabilization of the tracking line with respect to the line of sight depends on the speed of response, or band width of the tracking loop.

The tracking loop performance may be improved by addition of a single degree of freedom gyro. (Ref. 8) Two advantages are obtained by use of a gyro:

1. More accurate stabilization is possible in the presence of base motion.
2. The tracking line can be rotated with respect to the star-fixed co-ordinate system with a velocity proportional to a command signal.

The latter property permits acquisition of objects at altitude or, re-acquisition of an object lost to view momentarily.

One experiment of interest to astronomers is the measurement of stellar scintillation from the ground to high altitude. This can be accomplished by using a reflector telescope with a photoelectric photometer at the focus. Roll stabilization is not required, since the photomultiplier observes a circular area about the optical axis.

For this type of system the stabilization tolerance is considered sufficiently large that gyros are not necessary.

Detailed information on balloon behavior was not available. It was estimated that, during ascent, the balloon gondola would oscillate with a low frequency and a small amplitude.

A stabilization system was constructed for an instrument case of the type described. The problem of gimbal articulation was studied in order to achieve satisfactory stabilization with reasonably small torque motors.

One loop, the traverse system, was constructed from available parts. Static and dynamic analysis of the individual components and the loop were made. Compensation was designed using root locus techniques.

A two-axis system was constructed for quantitative performance evaluation. A complete analysis was not possible due to lack of time, but the experiments performed indicated that the system was satisfactory.

CHAPTER 2

GIMBAL ARTICULATION AND TORQUE MOTOR REQUIREMENTS

Two of the previously discussed image stabilization methods require gimbaling of the instrument case with respect to the base. Figure 2.1 illustrates support of the astronomical instrument with two gimbals identified as train and elevation gimbals. This configuration is suggested since the axis of symmetry of a balloon system is coincident, on the average, with the local vertical. Orientation of the telescope is based on training about the train (vertical) axis and elevating about an axis normal to the train axis. Yaw motion of the base will disturb the instrument case only through frictional coupling in the train gimbal bearing. Roll and pitch motions of the base will produce disturbing torques through radial bearing loads. These torques would be counteracted by the elevation and train drive motor torques generated in response to indicated angular deviations of the instrument case. The torque motors are the direct torque type. Accurate stabilization of the instrument would be more difficult if gear trains were used because of gear train inaccuracies and interfering torque coupling. The latter phenomena can be explained by considering that the train gimbal, for example, is driven through a gear train by a motor mounted on the base. Base rotation about the train axis would produce a torque on the train gimbal acting about the train axis because of gear train acceleration.

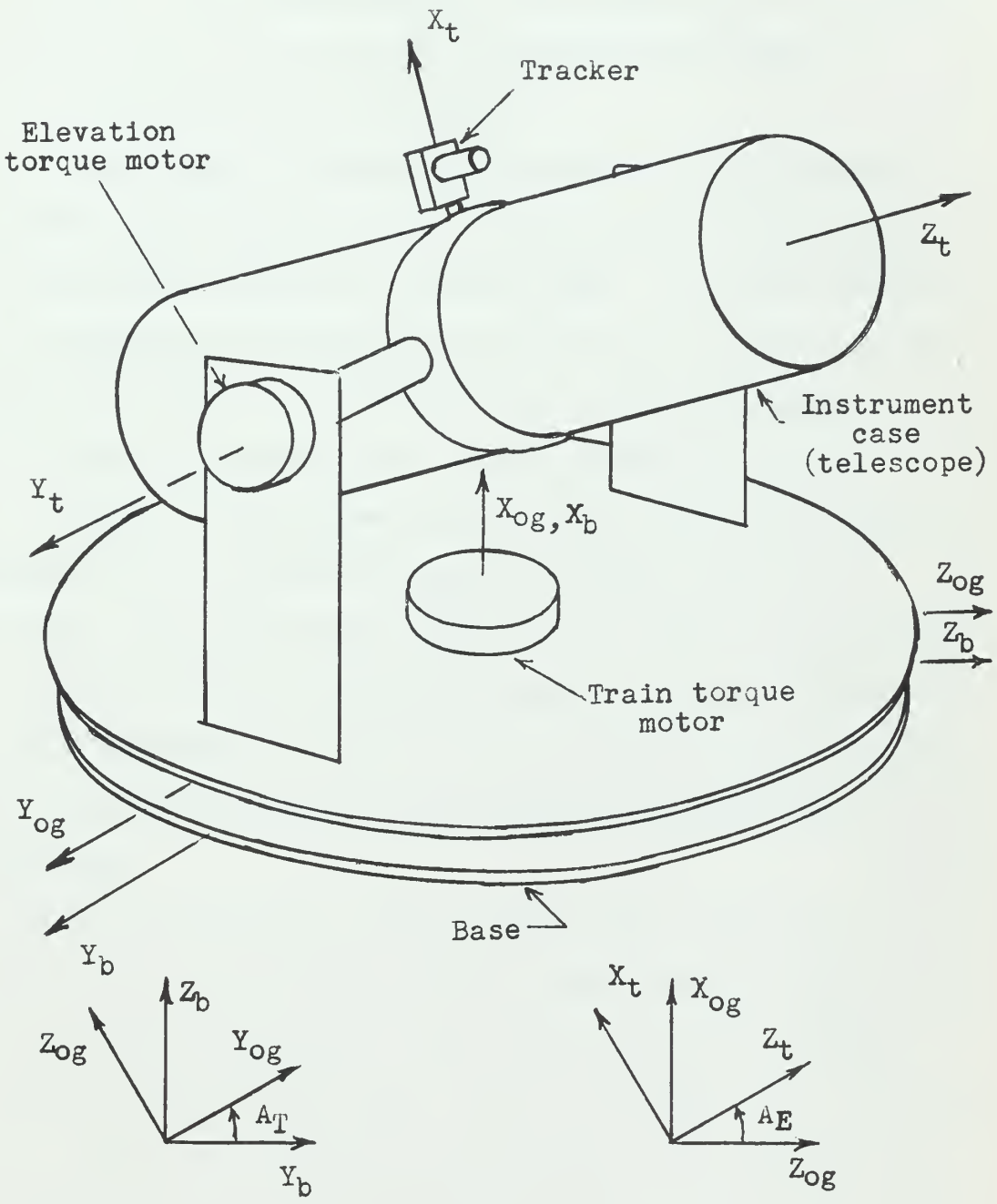

Figure 2.1 Two gimbal instrument mounting.

Derivation Summary 1 shows the expressions for angular velocities and torque caused by an interfering torque on a two-gimbal system due to base motion. From this derivation it can be seen that if the system is in perfect balance and no friction is present in the bearings, no torque is required about the elevation axis.

A disadvantage of the two-gimbal system becomes apparent if the elevation angle between the optical axis and the train axis changes by more than approximately 45° during the flight. It has been assumed that the misalignment of the optical axis and the line of sight is sensed by a device mounted on the instrument case, consequently angular correction data are generated in a traverse-elevation co-ordinate system. In Figure 2.1 the traverse axis would be fixed with respect to the instrument case and normal to both the elevation axis and the optical axis. Torque generation, based on these angular correction data, occurs in a train-elevation co-ordinate system, and co-ordinate transformation is necessary in order that the relationship between traverse angular deviations and attendant train torque be invariant to the elevation angle.

Figure 2.2 illustrates a three-gimbal system. Here the instrument case is supported by a traverse gimbal which, in turn, is supported by the elevation gimbal. The requirement for co-ordinate transformation has been eliminated. The train torque motor serves two purposes: First it is used to keep the instrument case centered in the inner gimbal and second it shares the load on the traverse torque motor due to interference torques and reduces the size requirement for the traverse torque motor. The train torque motor is driven by a signal from a potentiometer geared to the traverse drive shaft. The response time of the train system can be made longer than that of the traverse

DERIVATION SUMMARY 1

ANGULAR VELOCITY AND TORQUE EQUATIONS FOR A "PERFECT" TWO-GIMBAL SYSTEM

See Figure 2.1.

Subscripts are defined as follows:

t, telescope tube axis system

og, outer gimbal axis system

b, the bottom plate or base axis system

E, elevation

T, traverse

For purposes of this analysis, origins of all axis systems are coincident.

Equations can be written in two ways:

1. Co-ordinate transformation of telescope angular velocity into base angular velocity.

2. Co-ordinate transformation of base angular velocity into telescope angular velocity.

Boundary conditions:

1. The telescope optical axis is fixed in inertial space; that is, $W_{X_{(t)}} = W_{Y_{(t)}} = 0$.

No restrictions are placed on $W_{Z_{(t)}}$.

2. The base motion input is of the form

$$W_{X_{(b)}} = W_{Y_{(b)}} = 0 \qquad W_{Z_{(b)}} = \omega A \cos \omega t$$

This input was chosen as representative of the type of oscillation encountered by balloon gondolas.

EQUATION SET 1

From Figure 1:

$$W_{X_{(og)}} = W_{Z_{(t)}} \sin A_E$$

$$W_{Z_{(og)}} = W_{Z_{(t)}} \cos A_E$$

$$0 = W_{Y_{(og)}} \cos A_T - W_{Z_{(og)}} \sin A_T$$

$$\omega A \cos \omega t = W_{Z_{(og)}} \cos A_T + W_{Y_{(og)}} \sin A_T$$

$$A_E = A_{E_{(t=0)}} - \int_0^t W_{Y_{(og)}} \, dt$$

$$A_T = \int_0^t W_{X_{(og)}} \, dt$$

Or alternatively:

$$W_{Z_{(b)}} = \omega A \cos \omega t$$

$$W_{X_{(og)}} = W_{Z_{(og)}} \tan A_E$$

$$W_{Y_{(og)}} = \omega A \cos \omega t \sin A_T$$

$$W_{Z_{(og)}} = \omega A \cos \omega t \cos A_T$$

$$W_{Z_{(t)}} = W_{X_{(og)}} \sin A_E + W_{Z_{(og)}} \cos A_E$$

$$A_E = A_{E_{(t=0)}} - \int_0^t W_{Y_{(og)}} \, dt$$

$$A_T = \int_0^t W_{X_{(og)}} \, dt$$

EQUATION SET 2

Torque Equations

1. Basic Euler's Equations:

$$M_{X_{(t)}} = I_{X_{(t)}} \dot{W}_{X_{(t)}} - \left[I_{Y_{(t)}} - I_{Z_{(t)}}\right] W_{Y_{(t)}} W_{Z_{(t)}}$$

$$M_{Y_{(t)}} = I_{Y_{(t)}} \dot{W}_{Y_{(t)}} - \left[I_{Z_{(t)}} - I_{X_{(t)}}\right] W_{Z_{(t)}} W_{X_{(t)}}$$

$$M_{Z_{(t)}} = I_{Z_{(t)}} \dot{W}_{Z_{(t)}} - \left[I_{X_{(t)}} - I_{Y_{(t)}}\right] W_{X_{(t)}} W_{Y_{(t)}}$$

$$M_{X_{(og)}} - M_{X_{(t)}} \cos A_E - M_{Z_{(t)}} \sin A_E = I_{X_{(og)}} \dot{W}_{X_{(og)}} - \left[I_{Y_{(og)}} - I_{Z_{(og)}}\right] W_{Y_{(og)}} W_{Z_{(og)}}$$

$$M_{Y_{(og)}} - M_{Y_{(t)}} = I_{Y_{(og)}} \dot{W}_{Y_{(og)}} - \left[I_{Z_{(og)}} - I_{X_{(og)}}\right] W_{Z_{(og)}} W_{X_{(og)}}$$

$$M_{Z_{(og)}} + M_{X_{(t)}} \sin A_E - M_{Z_{(t)}} \cos A_E = I_{Z_{(og)}} \dot{W}_{Z_{(og)}} - \left[I_{X_{(og)}} - I_{Y_{(og)}}\right] W_{X_{(og)}} W_{Y_{(og)}}$$

2. By substitution from Equation Set 1:

$$M_{X_{(t)}} = 0$$

$$M_{Y_{(t)}} = 0$$

$$M_{Z_{(t)}} = I_{Z_{(t)}} \dot{W}_{Z_{(t)}}$$

$$M_{X_{(og)}} = I_{Z_{(t)}} \dot{W}_{Z_{(t)}} \sin A_E + I_{X_{(og)}} \dot{W}_{X_{(og)}} - \left[I_{Y_{(og)}} - I_{Z_{(og)}}\right] W_{Y(og)} W_{Z_{(og)}}$$

The torque $M_{Z_{(t)}}$ represents a radial bearing load. The only torque motor requirement is $M_{X_{(og)}}$ or traverse torque. Assuming negligible friction in the gimbal bearings, no torque is required in elevation.

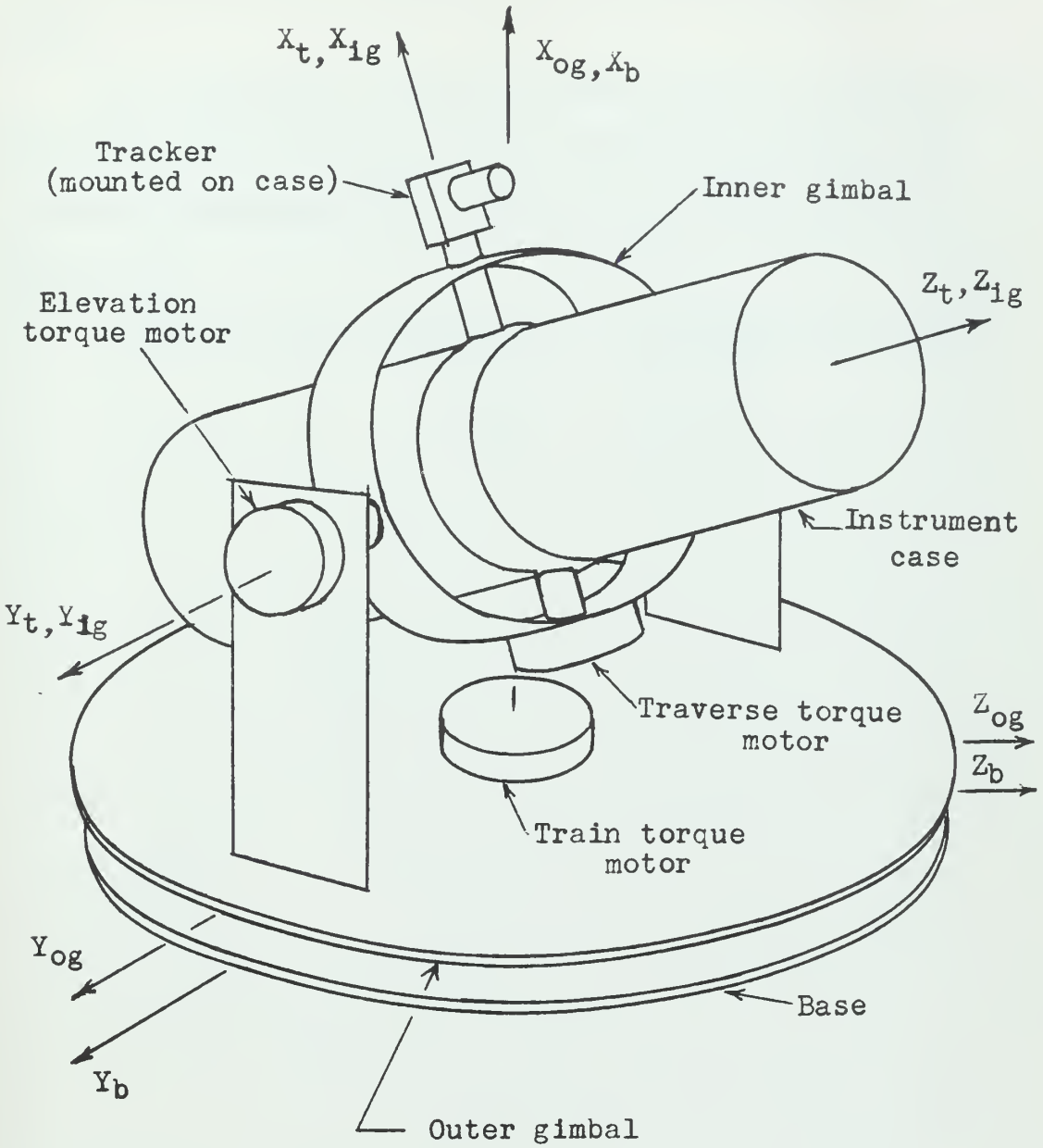

Figure 2.2 Three gimbal instrument mounting.

system to prevent oscillation due to coupling of the traverse and train drives.

Since this gimbal system effectively isolates the traverse and elevation modes, each system can be studied independently. The traverse system was studied experimentally to determine system performance.

Figure 2.3 shows a photograph of the experimental system.

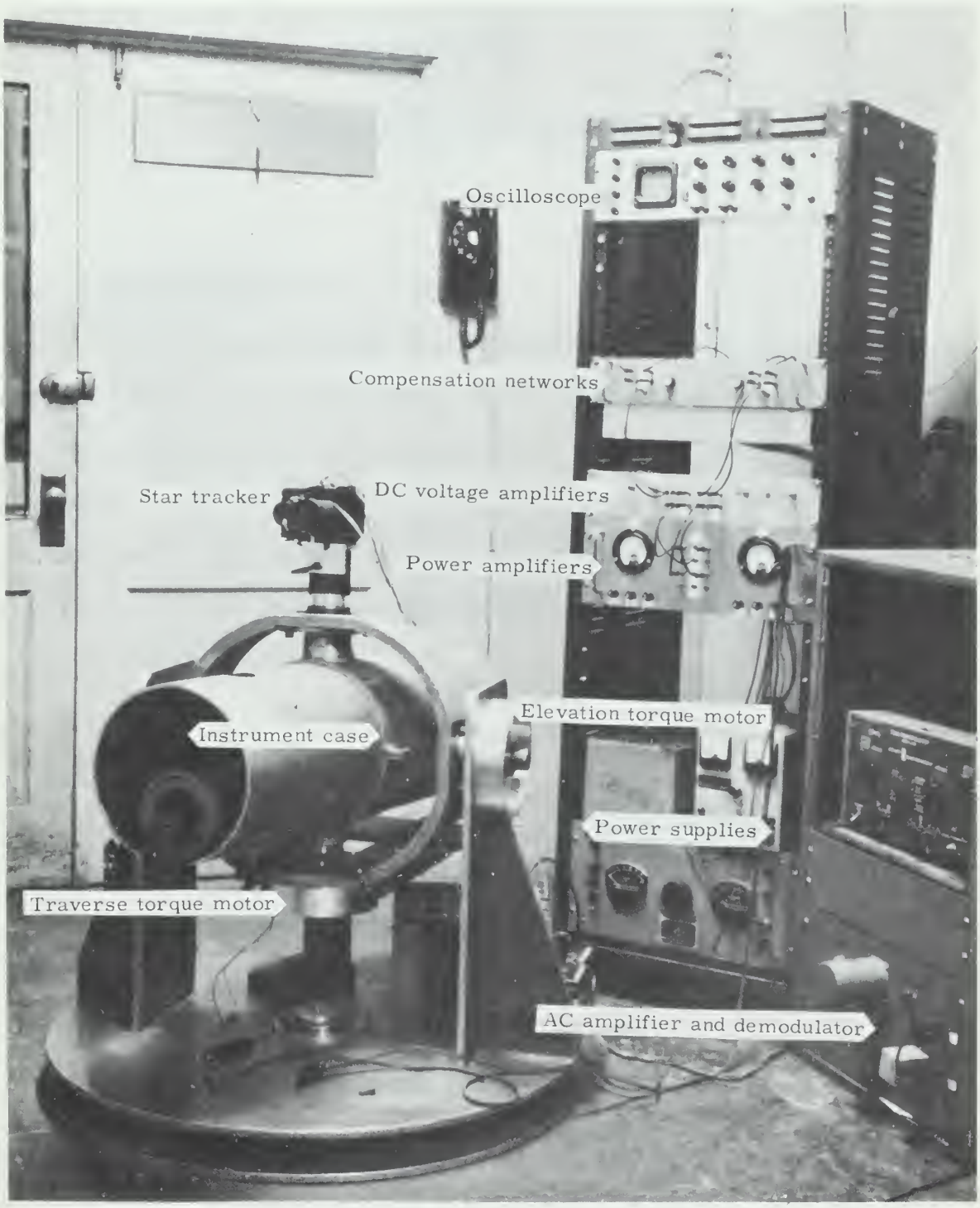

Figure 2.3 The Experimental Two-axis Stabilization System

CHAPTER 3

COMPONENT DESCRIPTION

3-1 THE EXPERIMENTAL SYSTEM

A functional diagram of the elevation and traverse servo loops for the balloon borne telescope is shown in Figure 3.1. The experimental system consisted of a telescope tube as the controlled member mounted in a gimbal system with torque motors on the bearing axes, a star tracker mounted on the telescope tube for error sensing, and appropriate electronics to complete the loops between the star tracker and the torque motors.

3-2 STAR TRACKER

The star tracker (Figure 3.2) uses a refracting telescope with a 50 milliradian field of view. Light from a star is collected by the objective lens and focused in the plane of a semi-circular aperture. The light passing through the aperture is defocused before impinging on a dynode of a 1P-21 type photomultiplier tube.

The semi-circular aperture is rotated at 60 cps by a two-phase a-c motor. The rotating aperture chops the light, modulating the light intensity at 60 cps. The exact shape of the output wave form varies with the size of the image, but the fundamental frequency is 60 cps.

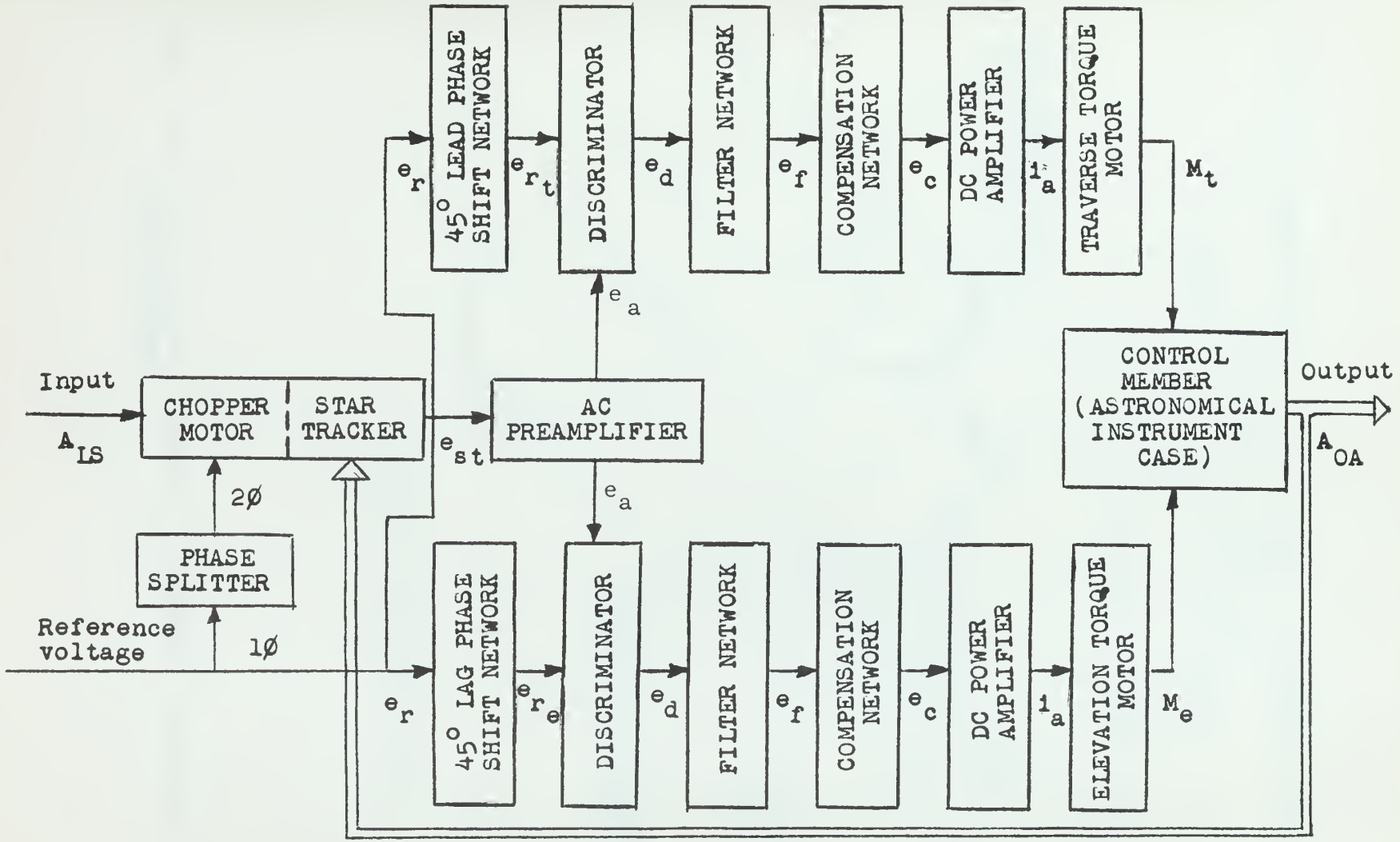

Fig. 3.1 Functional diagram of the traverse and elevation stabilization systems.

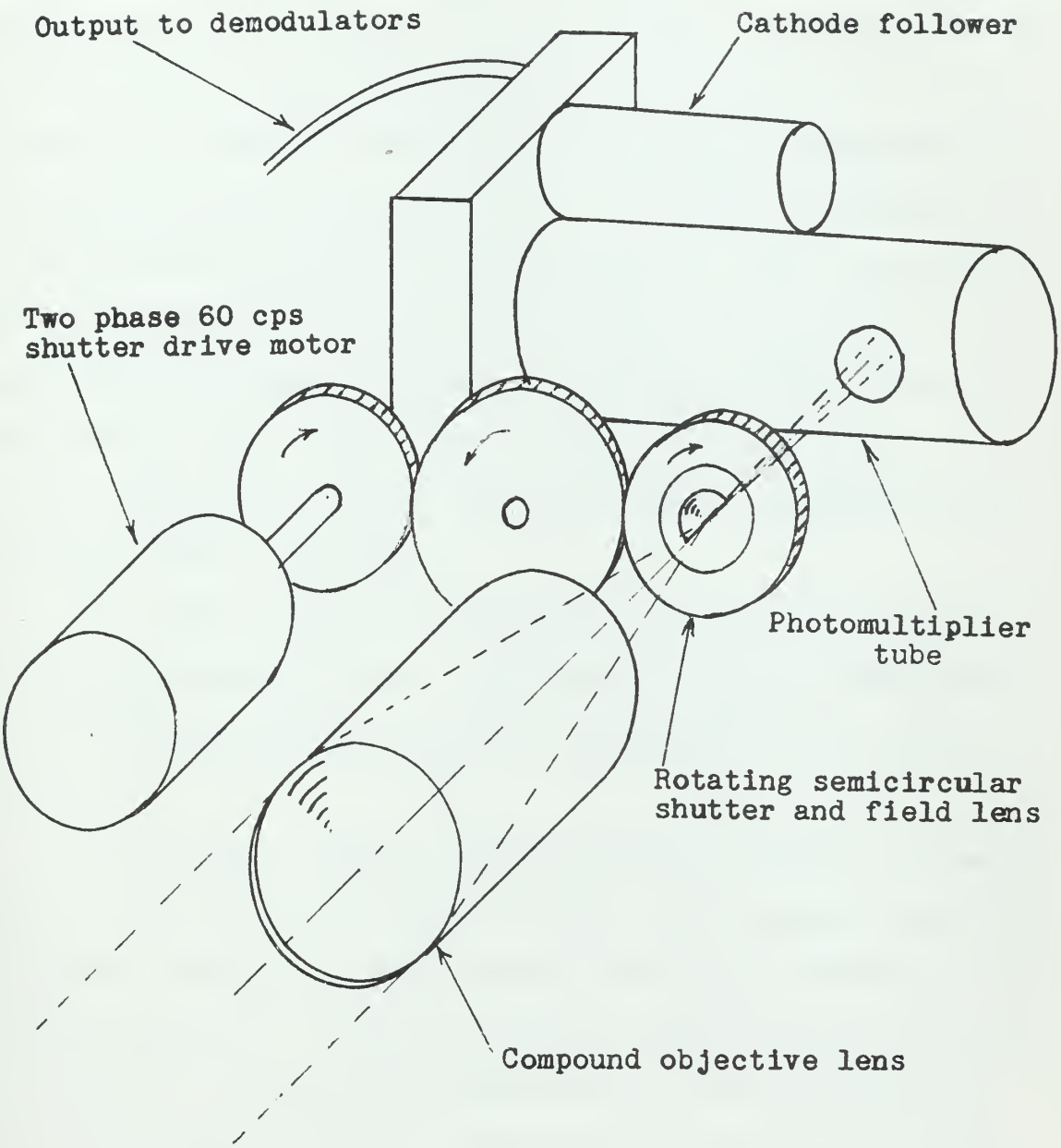

Fig. 3.2 Illustrative pictorial schematic diagram for the star tracker

When the light image is in the center of the aperture, there is no modulation, since the intensity is uniform. As the image moves away from the center, a 60 cps wave form is produced. The output signal is proportional to the image displacement from the optical axis as seen in the plane of the shutter. The amplitude of the signal is proportional to the image distance from the optical axis. The phase of the signal can be interpreted as an indication of direction of the image in the shutter plane. The interpretation is accomplished by comparison of the signal output of the star tracker with the reference voltage that is applied to the shutter motor. Geometrical reference of the star tracker voltage to the traverse and elevation axes is accomplished by rotating the shutter motor case.

The output of the star tracker is put through a cathode follower to reduce the output impedance. The frequency response of the cathode follower was measured and found to be essentially flat from 20 cps to 7000 cps.

Typical static response curves for the star tracker are shown in Figure 3.3 for various test light intensities. The defocused image width for this set of curves was approximately .040 inches in diameter. The test light source was a three-volt miniature tungsten lamp at a distance of 200 inches. The slope of the linear portion of these curves is the sensitivity of the star tracker. The performance function of the star tracker may be treated as a sensitivity because the sampling time of the chopped light is small compared to the significant time constants of the system and the chopping frequency of 60 cps is very large as compared to the bandwidth of 3.6 cps (see Chapter 4) of the system.

Thus $[PF]_{st\,(A_{LS}:e_{st})} = S_{st}$

$= 0.8$ volts (rms) per milliradian

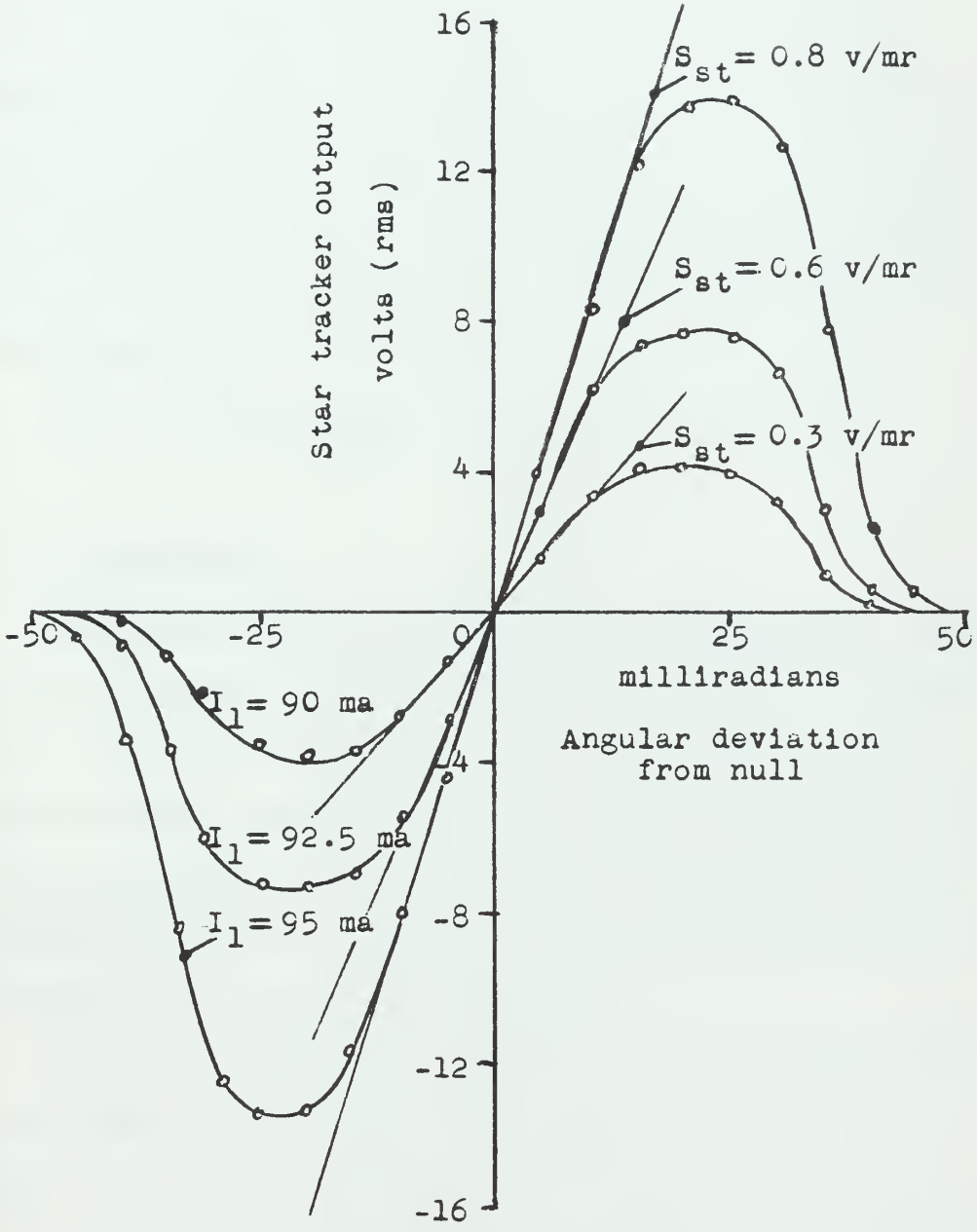

Fig. 3.3 Star tracker characteristics for various test light intensities.

3-3 AC PREAMPLIFIER

The AC preamplifier used was a high fidelity audio amplifier. It served as an impedance matching device to prevent the discriminator from loading the star tracker. As a matter of convenience the gain control in this amplifier was used to control the overall loop sensitivity of the system. The performance function of the pre-amplifier is treated as a sensitivity because it is only required to pass a narrow band of frequencies centered around the modulation frequency of 60 cps. The frequency response of the preamplifier was flat from 20 cps to 20,000 cps.

Thus $[PF]_{a(e_{st}:e_a)} = S_a$ volts per volt (rms)

3-4 DISCRIMINATOR

The discriminator is a phase sensitive demodulator. The phase reference of the discriminator was referenced to a single direction in the star tracker so that elevation and traverse signals could be isolated to drive the appropriate torque motors. The output of the discriminators was a full wave rectified a-c signal with a 120 cps fundamental frequency. A Polytechnic PRD type 808 ring diode demodulator was used for the discriminator.

Figure 3.4 shows the response curve of the discriminator for a signal that is in phase or 180° out of phase with the reference voltage. The performance function of the discriminator will be treated as a sensitivity because its dynamic characteristics are dependent on the filter that follows.

Thus $[PF]_{d(e_a:e_d)} = S_d$

$= 0.5$ volts (d.c.) per volt (rms)

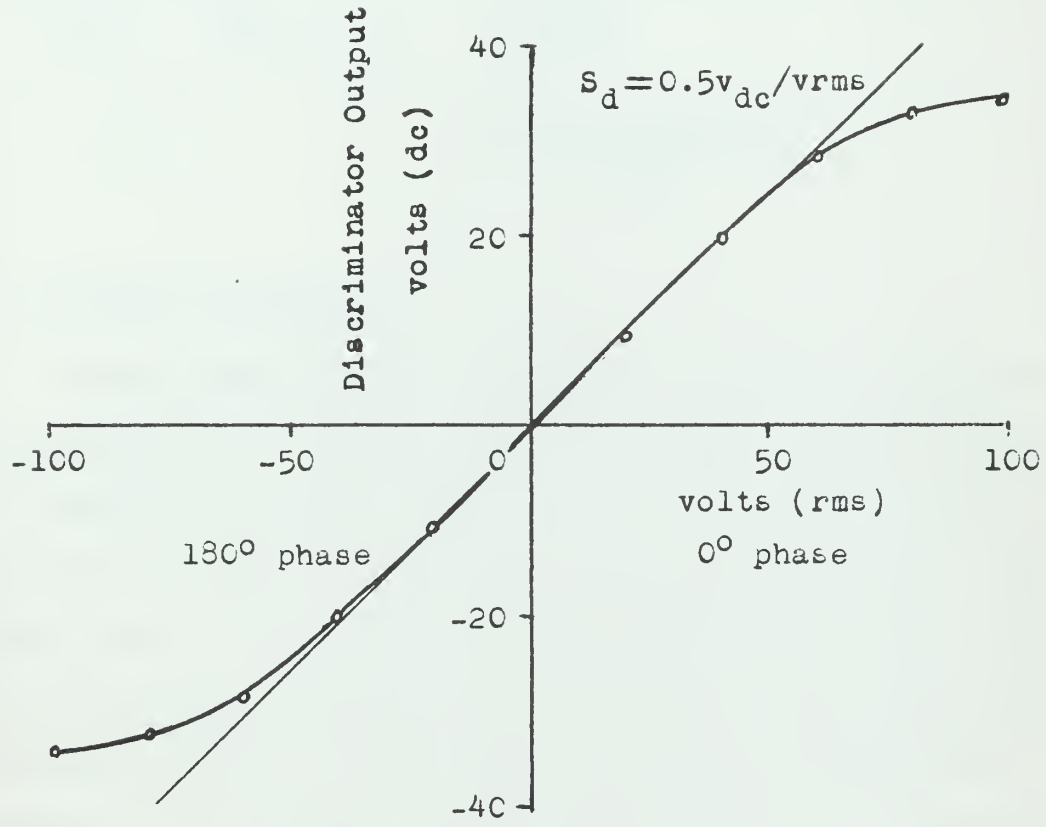

Fig. 3.4 Discriminator characteristics showing signal in phase and 180° out of phase with reference.

3-5 FILTER

Filtering was accomplished by a low pass RC passive network. The filter design was a compromise between minimization of the rms ripple voltage and minimization of a time constant in the servo loop. The ratio of rms ripple voltage to DC voltage was 0.2. The frequency response of the filter network with the previous components and the equivalent loading of a compnesation network is shown in Figure 3.5.

Thus $$[PF]_{f\,(e_d:e_f)} = \frac{S_f}{1 + T_f p}$$

$$= \frac{0.4 \text{ volts per volt}}{1 + \frac{p}{200}}$$

3-6 DC POWER AMPLIFIER

The DC power amplifier consisted of a high gain transistorized voltage amplifier that drives a bridge type current amplifier. The DC power amplifier is designed to deliver four to seven amperes into a low impedance of three to five ohms. Figure 3.6 shows the DC power amplifier static characteristics working into a seven-ohm load, which is the equivalent resistance of the torque motor. The frequency response of the power amplifier with its power supplies was measured with a servoscope. The response curve is shown in Figure 3.7. The power amplifier can be considered as a first order system.

Thus

$$[PF]_{p\,(e_f:e_p)} = \frac{S_p}{1 + T_p p}$$

$$= \frac{160 \text{ volts per volt}}{1 + \frac{p}{140}}$$

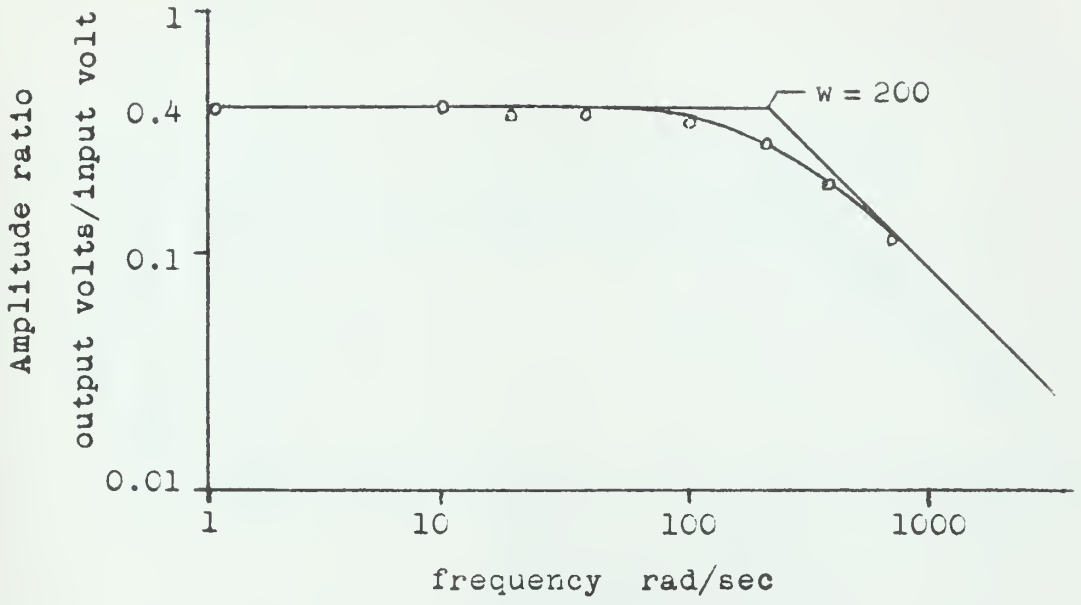

Fig. 3.5 Filtering network characteristics.

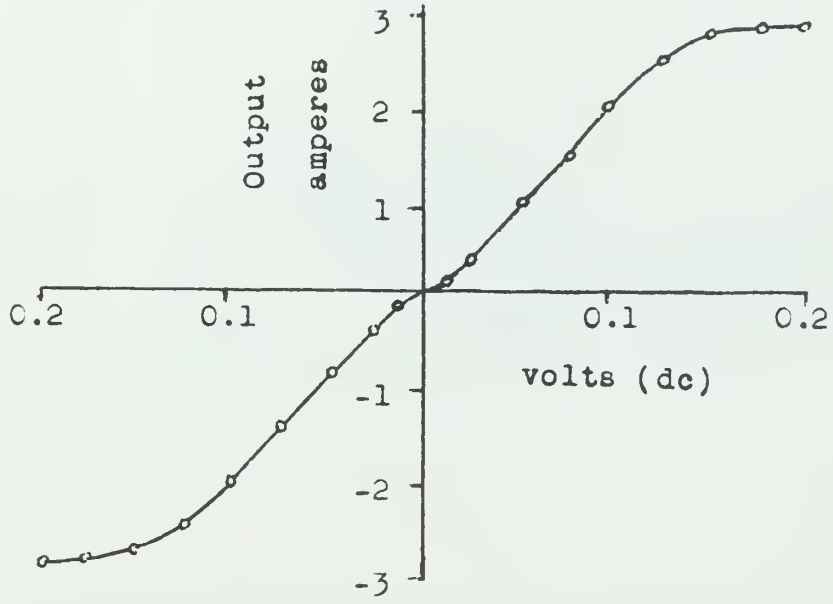

Fig. 3.6 DC power amplifier static characteristics for 7 ohm load.

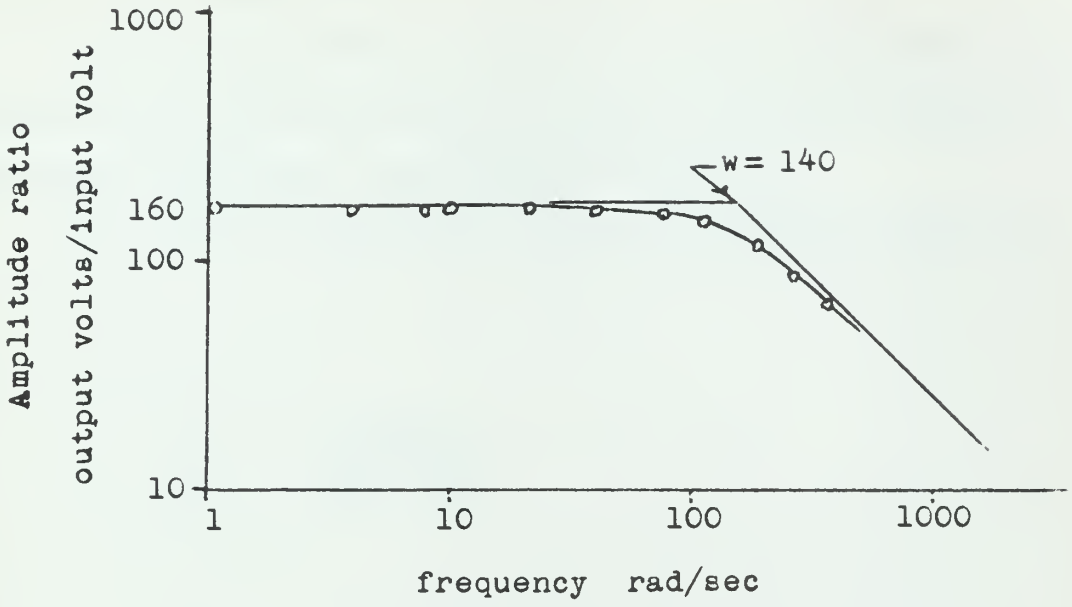

Fig. 3.7 DC power amplifier characteristics.

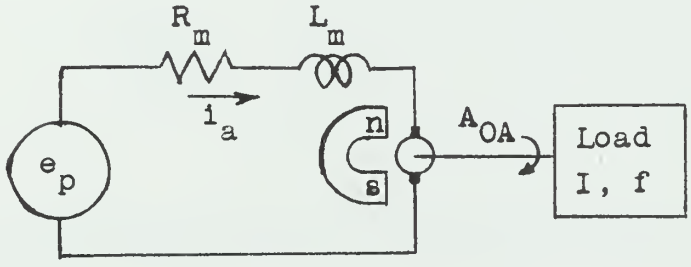

Fig. 3.8 Motor schematic with load.

3-7 DC TORQUE MOTOR

The DC torque motor is a direct drive permanent magnet type. The following torque motor analysis assumes linearity of electrical and magnetic parameters. See Figures 3.8 and 3.9.

The Laplace transformed equations describing the motor are

$$i_a = \frac{e_p - e_b}{L_m p + R_m}$$

$$M = k_t i_a$$

$$A_{OA} = \frac{M}{Ip^2 + fp}$$

$$e_c = k_v p A_{OA}$$

Combining these equations gives the performance function of the DC torque motor:

$$[PF]_{m(e_p:A_{OA})} = \frac{k_t}{p\left[(L_m I)p^2 + (R_m I + L_m f)p + k_v k_t + fR_m\right]}$$

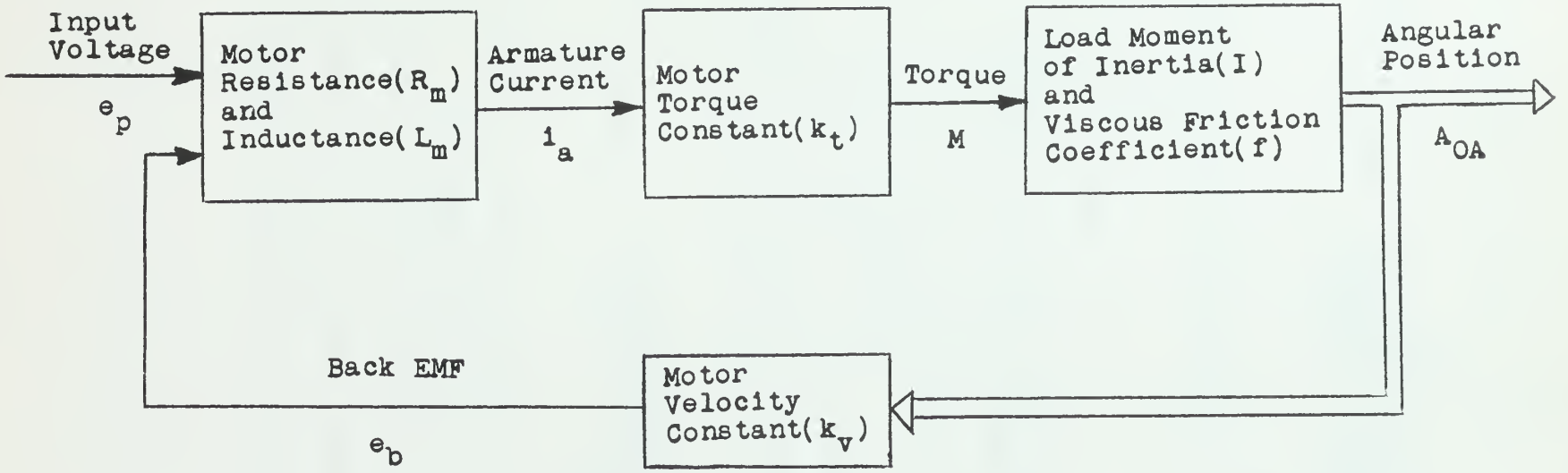

Fig. 3.9 Functional diagram of torque motor with load.

The viscous friction coefficient (f) is assumed to be negligible compared to the other parameters. Then

$$[PF]_{m(e_p:A_{OA})} = \frac{1/k_v}{p\left[\left(\frac{L_m I}{k_v k_t}\right)p^2 + \left(\frac{R_m I}{k_v k_t}\right)p + 1\right]}$$

The measured constants of the motor are

R_m = 7 ohm

L_m = 0.03 henries

I = 2.25 slug-ft^2 (includes instrument case and equivalent inertias of astronomical instruments)

k_t = 1.5 lb-ft/ampere (see Figure 3.10)

k_v = 2.04 volts/radian/sec
(volts/rad/sec = 1.356 × sensitivity in ft-lbs/amp)

The performance function for the torque motor including the inertia of instrument case and equivalent inertias of astronomical instruments is

$$[PF]_{m(e_p:A_{OA})} = \frac{0.5 \text{ radians/sec/volt}}{p\left(\frac{p}{0.1} + 1\right)\left(\frac{p}{230} + 1\right)}$$

Figure 3.11 shows the open loop response of the power amplifier and torque motor. In the range of frequencies used it shows that the motor has a second-order response. This was obtained by using a signal from a servoscope to drive the power amplifier and measuring the magnitude of angular deviation of the instrument case.

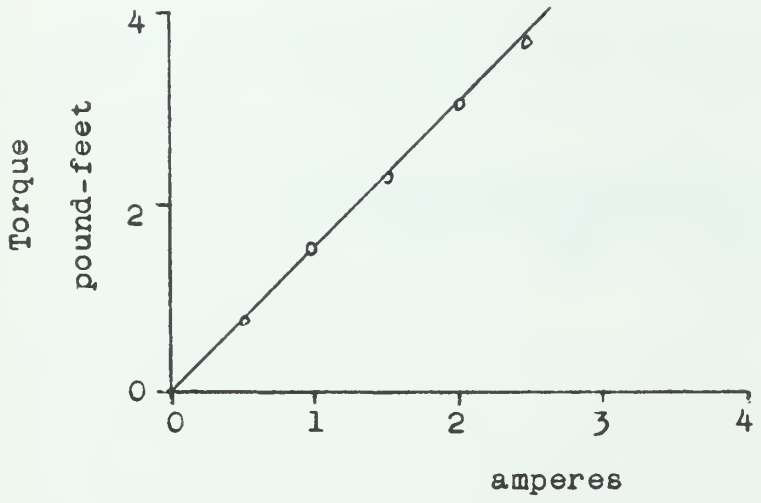

Fig. 3.10 Torque motor characteristics.

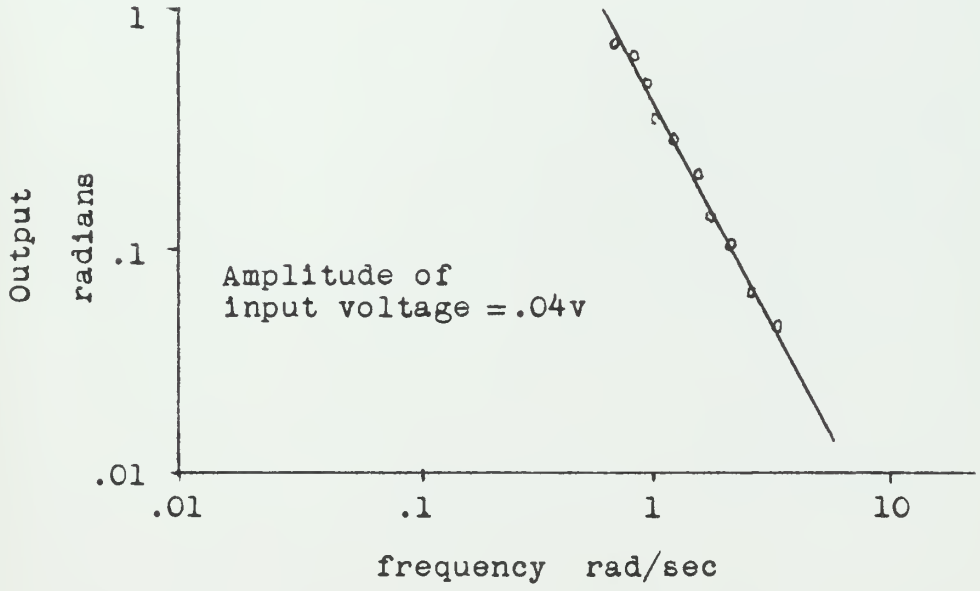

Fig. 3.11 Open loop response of power amplifier and torque motor with load.

3-8 OPEN LOOP PERFORMANCE FUNCTION

The open loop performance that now remains to be compensated before closing the servo loop is

$$[PF]_{OL} = [PF]_{st}\,[PF]_{a}\,[PF]_{d}\,[PF]_{f}\,[PF]_{p}\,[PF]_{m}$$

$$= \frac{11.5 \text{ radians/sec/milliradian}}{p\left(1+\frac{p}{0.1}\right)\left(1+\frac{p}{230}\right)\left(1+\frac{p}{140}\right)\left(1+\frac{p}{200}\right)}$$

CHAPTER 4

COMPENSATION

The design of the compensation network for the servo loop involved a compromise between the magnitude of error caused by interfering torques and the degree of stability. It is desirable to have as high a gain as possible to keep the magnitude of errors small and still maintain a stable system. Designing the network itself was inherently a trial-and-error process. The network used attenuated the low-frequency gain and therefore impaired the minimum error performance; yet increases in gain cancel this effect which decreased the degree of stability.

The open loop transfer function without compensation has five poles of which two have an immediate dominant effect on the stability. These two are located on and slightly to the left of the origin of the p-plane (see Figure 4.1). A slight gain of this uncompensated loop will immediately cause the system to go unstable. Therefore, it becomes necessary to insert a compensation network into the servo loop to improve its stability. A passive RC circuit lead network was selected which has a transfer function of

$$[PF]_{(e_{in}:e_{out})} = \frac{p+1}{p+11}$$

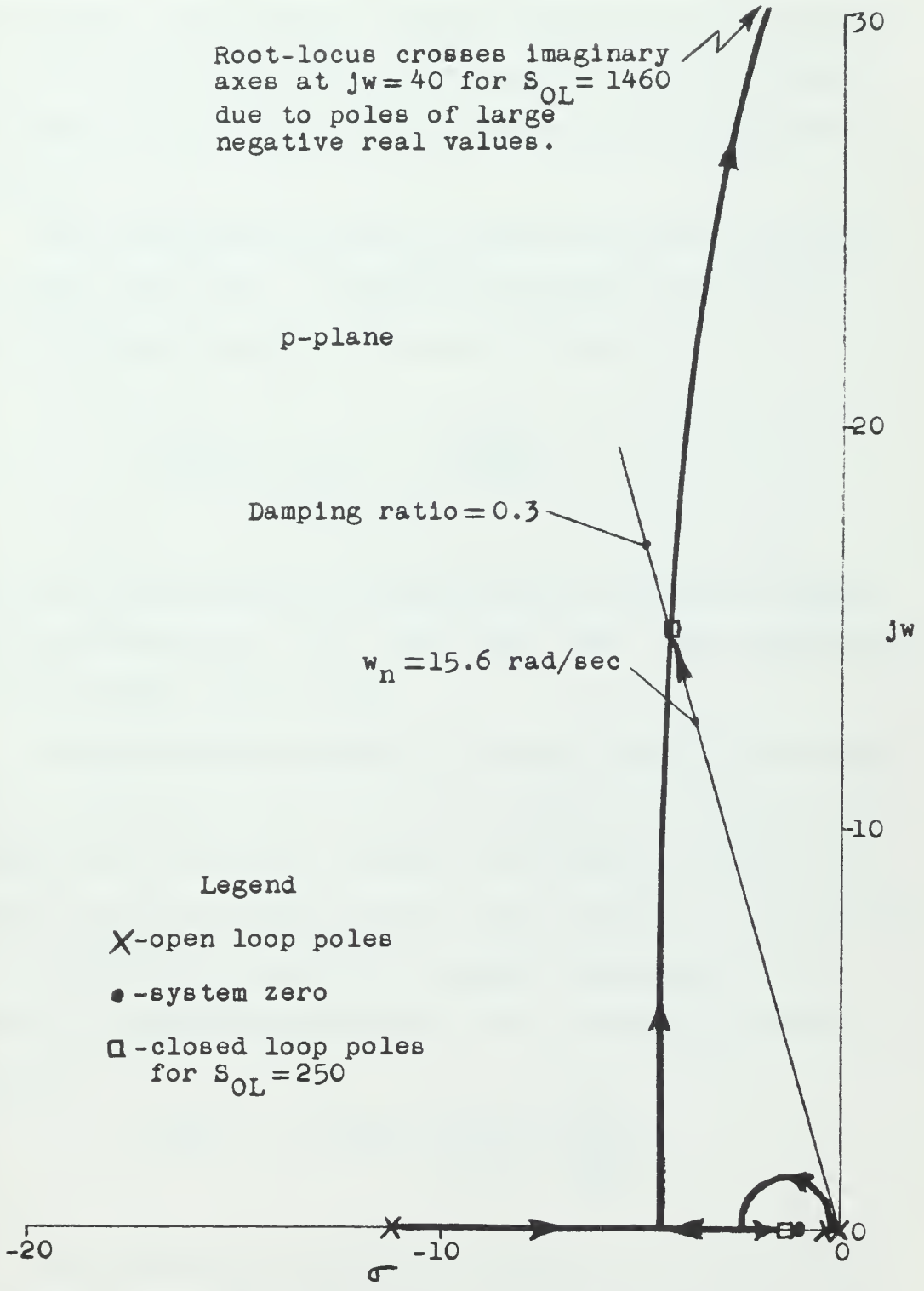

Fig. 4.1 Closed loop root-locus sketch showing only the dominate poles and zero.

The network is represented on the p-plane of Figure 4.1 by a pole at -11 and zero at -1. The zero near the origin keeps the root locus in the left hand plane, thus keeping the system stable for the lower values of gain. The ratio of pole distance to zero distance is made as high as practicable so that the pole will have minimum of cancelling effect on the zero.

Now it becomes necessary to improve the degree of stability for a higher value gain. An additional passive RC circuit lead network was placed in cascade. Its transfer function is

$$[PF]_{(e_{in}:e_{out})} = \frac{p + 67}{p + 267}$$

The zero of this network at -67 has the effect of delaying the lagging effect of the four poles at -140, -200, -230, -267. This stabilizes the system for higher values of gain.

These individual cascaded netwroks were inserted in the loop where the impedance which is seen by the network has minimum of loading on the filter and the impedance which loads the output of the network is at least ten times network output impedance. The cascading of the two individual networks has negligible loading effects on the networks. The performance function of the compensating network becomes

$$[PF]_c = 0.228 \frac{(1 + p)\,(1 + \frac{p}{67})}{(1 + \frac{p}{11})\,(1 + \frac{p}{267})}$$

The experimental results were obtained for an open loop gain setting (S_{OL}) of 250 (see Figure 4.1). For this gain one of the closed loop poles effectively cancels the zero at -1, thus leaving a dominant

pair of conjugate poles. The four poles at -140, -200, -230, -267 have negligible effect on the closed loop system. The system acts dynamically as a second order system with a damping ratio of 0.3 at a natural frequency of 15.6. The approximate closed loop performance function of the system becomes

$$[PF]_{CL} = \frac{1}{(1 + \frac{(2)(0.3)}{15.6}p + \frac{p^2}{(15.6)^2})}$$

Figure 4.2 shows the amplitude ratio and phase lag versus frequency of this closed loop system. It has a band width of 3.6 cps. The band width as used here is defined as the frequency range throughout which the amplitude response does not drop below 0.707 amplitude ratio.

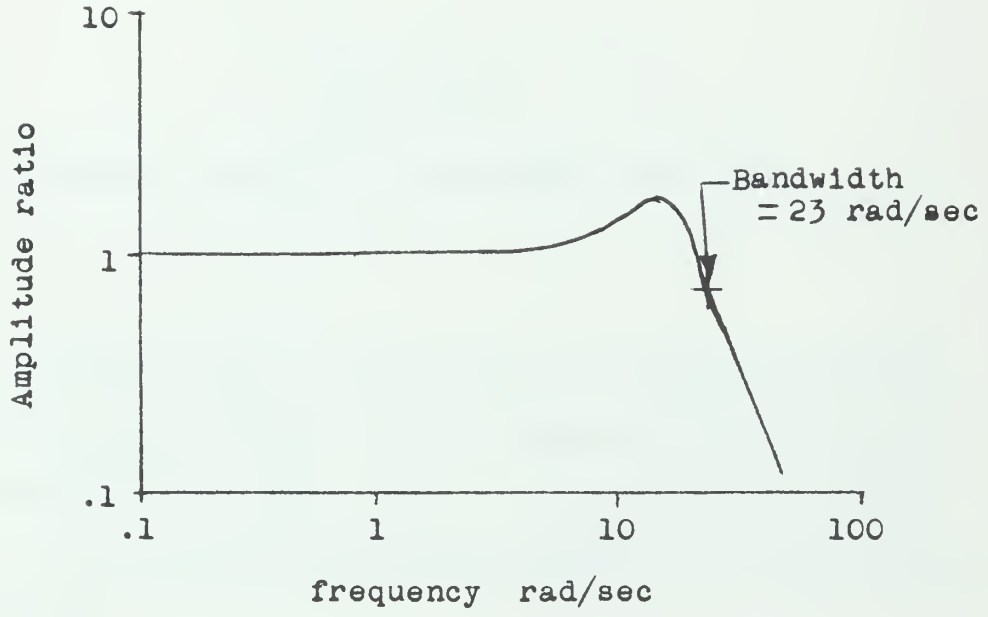

Frequency response

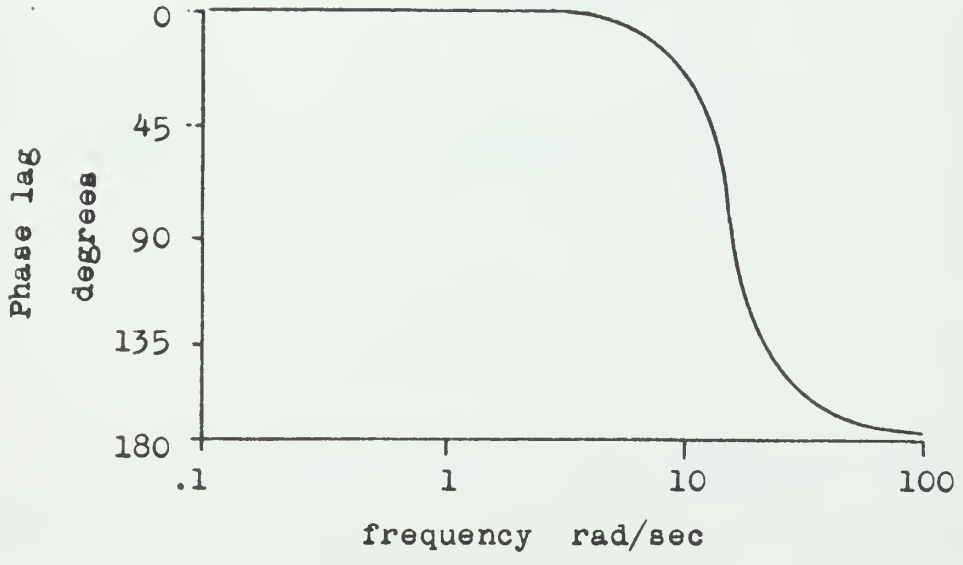

Fig. 4.2 Closed loop system characteristics.

CHAPTER 5

ERRORS CAUSED BY INTERFERING TORQUES

A source of error introduced into the system is caused by interfering torques transmitted to the telescope through the gimbals and bearing friction by base motion. An analysis of this error is made by considering the mathematical diagram of the system shown in Figure 5.1.

Where

$$[PF]_{(A_{LS} - A_{OA}:e_p)} = [PF]_{st}\,[PF]_a\,[PF]_d\,[PF]_f\,[PF]_c\,[PF]_p$$

$$\simeq \frac{.525\,(1+p)}{(1+\frac{p}{11})}$$

and

$$[PF]_{(e_p - e_b:M)} = \frac{k_t}{L_m p + R_m}$$

$$\simeq .214$$

Since the bandwidth of the system is narrow (see Chapter 4), it is reasonable to approximate the performance function by neglecting the dynamics in the components having time constants of less than .015 seconds.

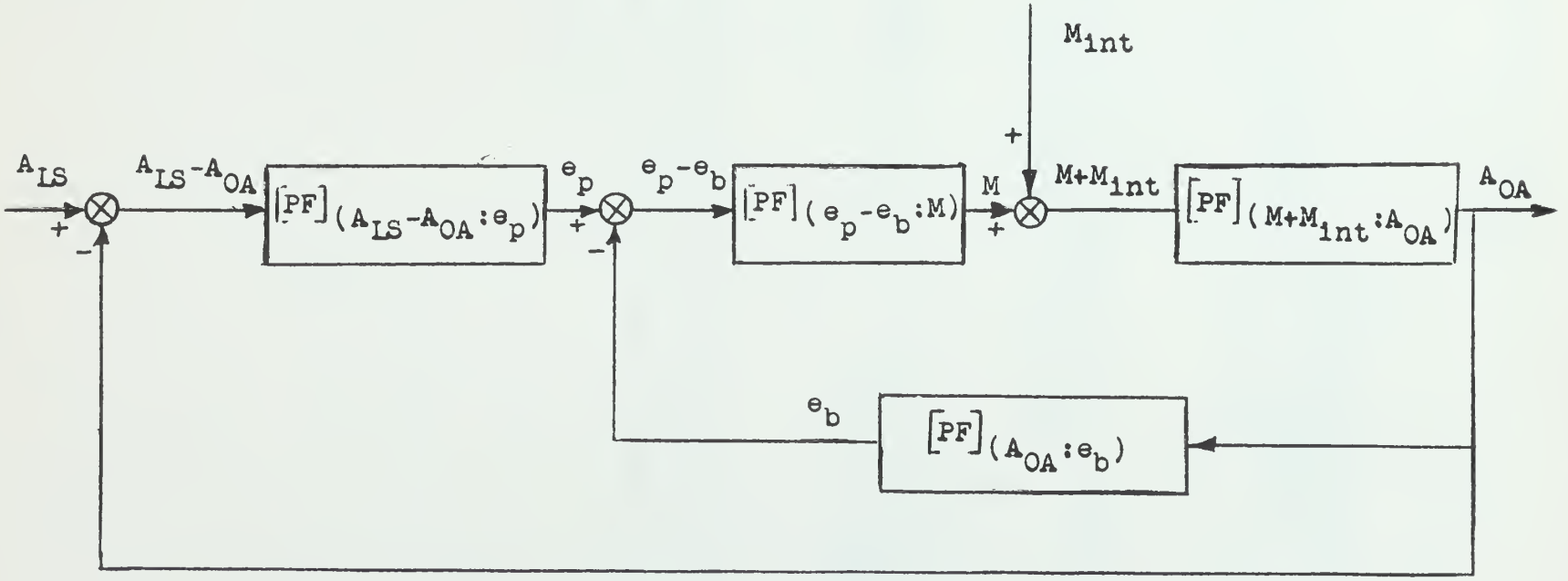

Fig. 5.1 Mathematical diagram of the system showing the interfering torque.

Since

$$[PF]_{(M_{int}:A_{OA})_{CL}} =$$

$$\frac{[PF]_{(M + M_{int}:A_{OA})}}{1-\left[[PF]_{(A_{OA}:e_b)}+[PF]_{(A_{LS}- A_{OA}:e_p)}\right]\left[[PF]_{(e_p-e_b:M)}[PF]_{(M+M_{int}:A_{OA})}\right]}$$

$$= \frac{1}{[PF]_{(A_{LS}-A_{OA}:e_p)}\,[PF]_{(e_p-e_b:M)}}\,[PF]_{(A_{OA}:A_{LS})\,CL}$$

Then

$$[PF]_{(M_{int}:A_{OA})\,CL} = \frac{8.7\,(1+\frac{p}{11})}{(1+p)\,(1+\frac{(2)(0.3)}{15.6}\,p+\frac{p^2}{(15.6)^2}}$$

Figure 5.2 shows a plot of the above performance function of milliradians in angular error per interfering torque in pound-feet versus frequency.

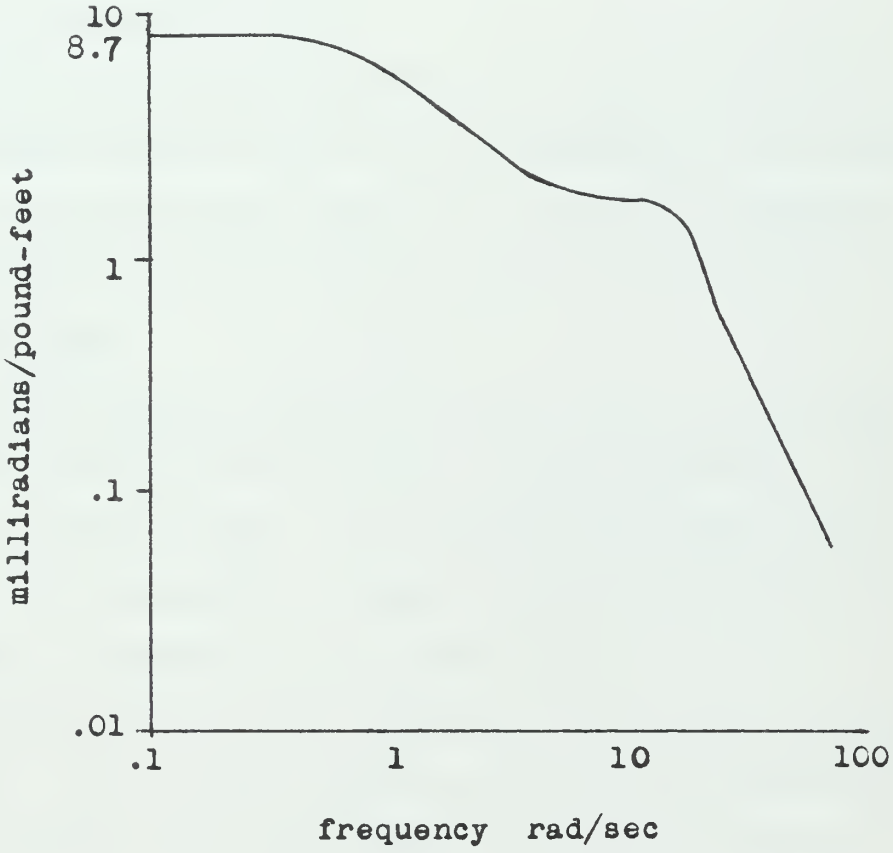

Fig. 5.2 Angular deviation per interfering torque versus frequency.

CHAPTER 6

EXPERIMENTAL RESULTS

6-1 STATIC PERFORMANCE

Measurement of static system error was accomplished by use of a dial gauge mounted on the base with the sensing element making contact with the instrument case in such a manner that angular displacements of the instrument case were read as linear displacements of the dial gauge.

With the system locked on the light source, the instrument case was forced off the line of sight to the star and released. This was done in both directions. The average distance between the static positions after disturbance, or dead zone, was determined to be 0.3 milliradian or approximately one minute of arc.

Static sensitivity of the system was 0.115 ft-lb/mr beyond the dead zone. A plot of static sensitivity showing torque generated as a function of displacement of the optical axis is shown in Figure 6.1.

6-2 DYNAMIC PERFORMANCE

The frequency response was calculated analytically as shown in Chapter 4. A plot of the calculated frequency response is shown in Figure 4.2.

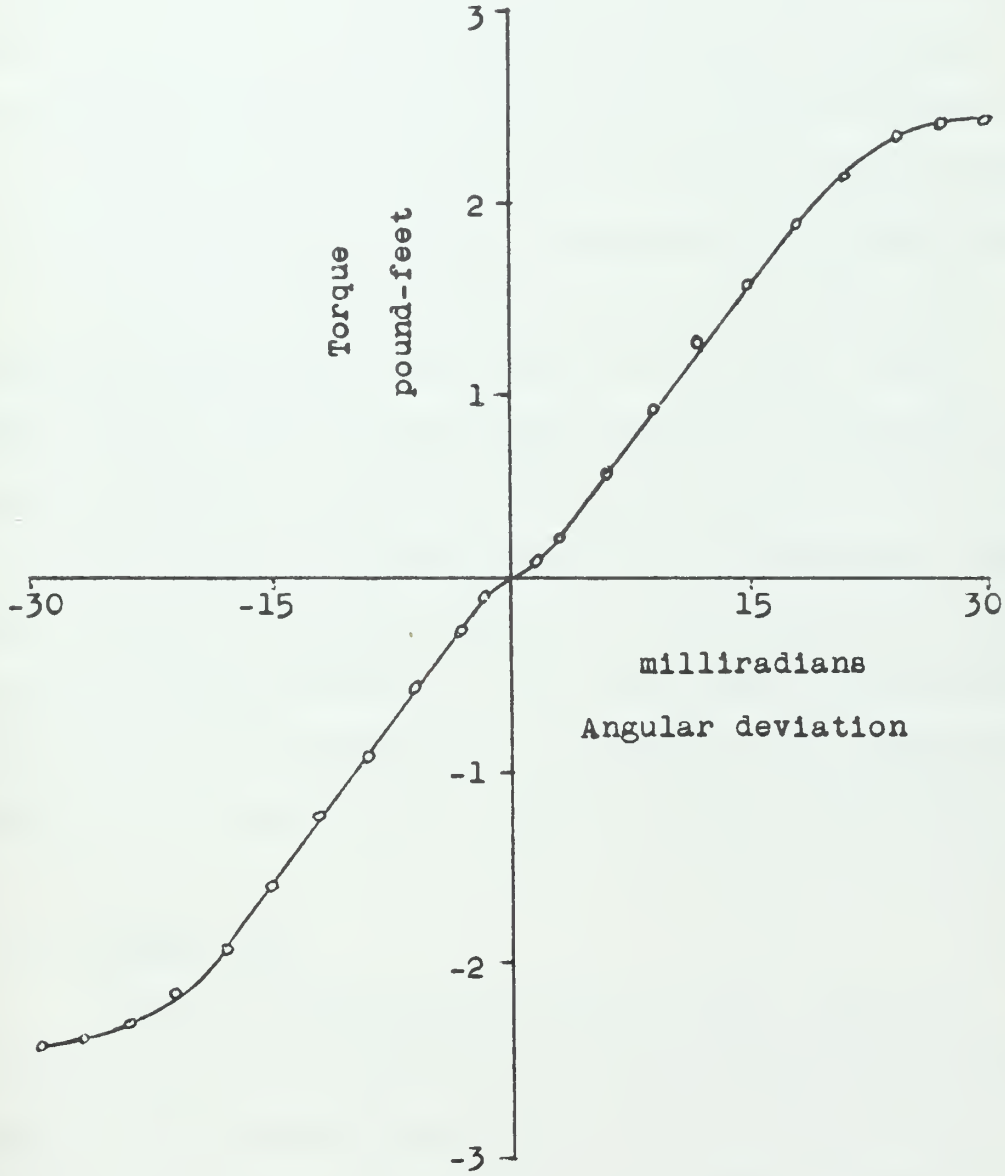

Fig. 6.1 Static characteristics of torque versus angular deviation of experimental system.

An identical stabilization system was constructed for the elevation loop. In order to test the tracking ability of the two-axis system, a test light was mounted on an arm rotated first in a vertical plane, parallel to the line of sight from the star tracker. Cross coupling between the elevation and the traverse loops could then be noted, since only the elevation loop should respond to the light. No traverse output was observed, hence it was concluded that there was no cross coupling. The light was then rotated in a plane perpendicular to the line of sight. The telescope tracked the light satisfactorily.

Tests were made to determine if the star tracker could track second magnitude stars, Polaris in particular. Results indicated that a useful signal could be generated. Observations were made on the roof of the M. I. T. Instrumentation Laboratory with a full moon with background lighting from the city of Cambridge. Under these conditions the signal-to-noise ratio of the output of the star tracker was approximately 1. 6. The output signal was considerably less than the signal obtained from the test light in the laboratory. The signal can be brought up to the required level by amplification.

6-3 SYSTEM NOISE

There were three major sources of noise. The most prevalent noise was caused by stray pickup and nonregulated power supplies. The second source of noise was the photomultiplier tube. The third source was due to the mechanical shutter drive in the star tracker. Noise is treated here because of the serious limitations that it places on the performance of the system.

The error signal is modulated at 60 cps. For this reason, the entire system required extensive shielding from the laboratory 60 cps

power source. All power to the star tracker with the exception of the shutter motor was supplied by batteries. As a result, the pickup was reduced to 0.001 volts rms at the output of the cathode follower. The power supplies for the power amplifier were either batteries or extremely well regulated DC power supplies.

In order to obtain a usable output signal from a star, a highly photo-sensitive device is required. For this reason, the 1P-21 photomultiplier tube was used. Nine photomultiplier tubes were tested against the same source for rms values of dark noise and peak signal at a deflection of 20 milliradians from null. All values were measured at the output of the cathode follower. The light source was a three-volt miniature tungsten lamp supplied with 92.5 milliamperes of current.

A signal-to-noise ratio based on the ratio of peak signal to noise at null was computed for each tube and tabulated in Table 6.1. The photomultiplier tube with the lowest dark noise level of .02 volts rms was used for the experiment. It had a signal-to-noise ratio of nine. The dark noise of the photomultiplier is random with sharp peaks.

An amplitude spectrum analysis of the dark noise and signal at null of a photomultiplier tube is shown in Figure 6.2. The spectrum was obtained by photographing the screen of a Panoramic Sonic Analyzer for a period of 25 sweeps, in order to average the random peaks. The photographs indicated that the noise peaks at 60 cps and drops off smoothly to 20,000 cps. It shows that the rms value at null is five times the rms value of dark noise for the tube which was used in the experiment.

The third source of noise was caused by the mechanical shutter drive in the star tracker. If the bearings were not properly

TABLE 6.1

Photomultiplier Tube Characteristics

Tube No.	Dark Noise (RMS Volts)	Signal Output (RMS Volts)	Signal/Noise Ratio
1	.040	4.0	100
2	.040	0.15	3.8
3	.060	1.00	16.7
4	.030	0.15	5.0
5	.030	0.11	3.7
6	.020	0.18	9.0
7	.025	0.14	5.6
8	.024	0.14	5.8
9	.043	0.30	6.8

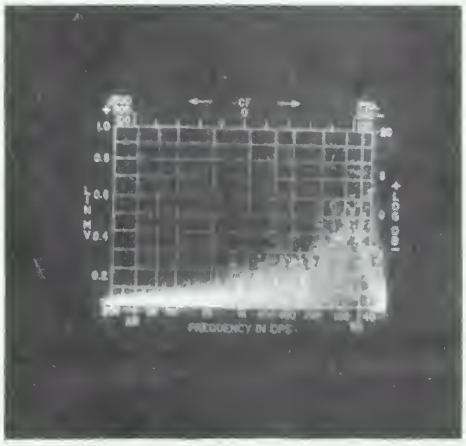

Linear voltage scale 0.1v
RMS volts = .15

Dark Noise

Linear voltage scale 1.0v
RMS volts = .75

Null Noise

Fig. 6.2 Amplitude spectrum analysis of dark noise and signal at null of a 1P-21 photomultiplier tube.

lubricated or cleaned, the shutter gear would catch periodically, causing an apparent phase shift of the output signal. This apparent phase shift was sufficient to cause the system to lose the star.

CHAPTER 7

CONCLUSIONS AND RECOMMENDATIONS

A stabilization system suitable for scintillation studies can be constructed with existing equipment and techniques.

Gyros are not required to stabilize this system. However, the target must be acquired before launch. Obstructions, such as clouds or parts of the balloon system which obstruct the star tracker field of view, will cause loss of the target due to the absence of gyros.

Considerable improvement in system performance can be gained by improving the individual components. Star tracker sensitivity can be increased by the use of reflecting optics. Star tracker signal-to-noise ratio can be improved by modulation at a higher frequency and by use of a narrow band-pass filter. Particular care must be taken in the selection of the photomultiplier tube.

The system sensitivity can be improved by increasing the gain of the d.c. amplifier. Gains in the rest of the experimental system were limited by saturation limits on the demodulator and star tracker.

The dead zone can be decreased by improved biasing techniques in the transistorized power amplifier.

Interesting avenues of further study might include:

1. Closing the train loop and determining the frequency spread required between the traverse and train loops to

prevent induced oscillation.

2. Application of base oscillation to the system and measurement of the torque motor outputs to correlate with the equations in Derivation Summary 1.

3. Investigation of other loop compensation, including various types of feedback.

4. An analytical study of the three-gimbal system to determine optimum torque motor size for a balloon telescope system.

5. An analysis of the motion of a large, high altitude balloon system from sea level to altitude. This could be done by installing a gyro package with appropriate recording equipment aboard a balloon.

BIBLIOGRAPHY

1. Gibson, John E., and Franz B. Tuteur: Control System Components, 1958, McGraw-Hill Book Co., Inc., New York.

2. Savant, Jr., C. J.: Basic Feedback Control System Design, 1958, McGraw-Hill Book Co., Inc., New York.

3. "High-Performance Demodulators for Servomechanisms," Schreiner, Kenneth E., Proceedings of the National Electronics Conference, 1946, Vol. II, pp 393-403.

4. "Direct Drive Servo Control Using Inland Torque Motors," Smith, David C., Electromechanical Components and Systems Design, January-February, 1958.

5. Thaler, Geo. J., and Robert G. Brown: Servomechanism Analysis, 1953, McGraw-Hill Book Co., Inc., New York.

6. Terman, Frederick Emmons: Radio Engineers' Handbook, 1943, 1st ed., 8th imp., McGraw-Hill Book Co., Inc., New York.

7. Draper, Charles Stark, Walter McKay, and Sidney Lees: Instrument Engineering, Vol. III, 1955, 1st ed., McGraw-Hill Book Co., New York.

8. Packman, Paul Edward: An Automatic Star Tracking System, Master's Thesis, M.I.T., August, 1958.